Preprint Title	Topographic signatures and manipulations of Fe atoms, CO molecules and NaCl islands on superconducting Pb(111)
Authors	Carl Drechsel, Philipp D'Astolfo, Jung-Ching Liu, Thilo Glatzel, Rémy Pawlak and Ernst Meyer
Publication Date	23 Aug. 2021
Article Type	Letter
ORCID® iDs	Rémy Pawlak - https://orcid.org/0000-0001-8295-7241

Topographic signatures and manipulations of Fe atoms, CO molecules and NaCl islands on superconducting Pb(111)

Carl Drechsel[1], Philipp D'Astolfo[1], Jung-Ching Liu[1], Thilo Glatzel[1], Rémy Pawlak*[1] and Ernst Meyer*[1]

Address: [1]Department of Physics, Universität Basel, Klingelbergstrasse 82, 4056 Basel, Switzerland

Email: Rémy Pawlak - remy.pawlak@unibas.ch; Ernst Meyer - ernst.meyer@unibas.ch

* Corresponding author

Abstract

Background: Topological superconductivity emerging in one- or two-dimensional hybrid materials is predicted as a key ingredient for quantum computing. However, not only the design of complex heterostructures is primordial for future applications but also the characterization of their electronic and structural properties at the atomic scale using the most advanced scanning probe microscopy techniques with functionalized tips.

Results: We report on the topographic signatures observed by scanning tunneling microscopy (STM) of carbon monoxide (CO) molecules, iron (Fe) atoms and sodium chloride (NaCl) islands deposited on superconducting Pb(111). For the CO adsorption a comparison with the Pb(110) substrate is demonstrated. We show a general propensity of these adsorbates to diffuse at low temperature under gentle scanning conditions.

Conclusion: Our findings provide new insights into high-resolution probe microscopy imaging with terminated tips, decoupling atoms and molecules by NaCl islands or tip-induced lateral manipulation of iron atoms on top of the prototypical Pb(111) superconducting surface.

Keywords

Superconductivity, NaCl, CO, scanning tunneling microscopy, lateral manipulation

Introduction

The most exciting manifestation of topological superconductivity [1-3] is the Majorana zero mode (MZM), which has attracted a tremendous interest due to its non-Abelian quantum exchange statistics proposed as a key ingredient for topological quantum computing [4-6]. Topological superconductivity can intrinsically arise in the bulk of certain materials [7] or can be engineered at the interface between two materials, exhibiting particle-hole symmetry and spin-orbit interaction [8]. Among the most promising platforms to realize MZMs are semiconducting nanowires with large spin-orbit coupling [9-12] or atomic chains [13-18] in proximity to an *s*-wave superconductor. The realization of MZMs in two-dimensions has been also observed in vortex cores on a proximitized topological insulator surface [19,20], in iron-based superconductors [7,21,22] or hybrid van der Waals heterostructures [23]. The fingerprint for MZMs in conductance measurements through the nanowire or in scanning tunneling spectroscopy (STS) is a zero-bias conductance peak occurring at boundaries and defects. Unfortunately, other structural peculiarities can also mimick such zero-bias anomalies, which eventually leads to severe misinterpretations. Therefore, the latest advances in scanning tunneling microscopy (STM) and atomic force microscopy (AFM) are required to accurately disentangle structural and electronic properties of these MZMs platforms.

The development of functionalized tips, obtained by picking up a single molecule from a surface, has been an important milestone for low temperature STM/AFM techniques since the CO tip nowadays enables systematic high-resolution measurements of surfaces, molecules and atoms [24-26]. STM/AFM indeed allows controlled repositioning of adsorbates, both in vertical and lateral directions. Atoms and molecules can be pushed or pulled across a surface [27-29], but also picked up and dropped with the probing tip [30-33]. Lateral repositioning of adatoms is also an promising asset as it could serve as unique opportunity to design atomic structures with novel electronic properties [27,34,35].

It is however astonishing, that most recent advances in manipulation experiments or contrast enhancement with functionalized tips are hitherto at their infancy, when studying a superconducting surface by STM/AFM. Although the earliest proposal for observing MZMs suggested to reposi-

tion Fe adatoms one-by-one with an STM tip in an one-dimensional fashion on an *s*-wave superconductor [10], this strategy has been primarily postponed in favor of self-assembly processes on Pb(110) surfaces [14,15,36,37]. Only recently, the successful manipulation of tens of Fe atoms has been reported on superconducting Re(0001) [16] and Ta(100)-O surfaces [38]. Despite being well-established on many noble metals, the use of CO-terminated tips also remains quite scarce in the literature [28], which severely limits the use of AFM as imaging tool on superconductors.

Recently, Heinrich *et al.* have demonstrated the possibility to tune the magnetic anisotropy of a single porphyrin molecule by perturbing its ligand field with the STM probe [39,40]. These results not only suggest the importance of future manipulations experiments, but also shed new lights into the potential of decoupling atoms and molecules electronically from the underlying superconductors. With this prospect, we emphasize that in addition to tip manipulations the use of alkali-halide islands, adsorbed on a superconducting surface and acting as a buffer layer, is another interesting field for research on topological superconductors [41-44].

In this work, we report on the topographic features of adsorbed CO molecules, NaCl layers and iron adatoms on a superconducting Pb(111) surface, investigated with STM at 4.8 K. We show that CO molecules on Pb(111) are hardly visible in STM images due to their high diffusion induced by the tip even at low temperature. This differs slightly from the adsorption on Pb(110), which has also been performed. In contrast, NaCl islands and single Fe atoms are more stable. Nevertheless, a general propensity for a tip-induced displacement of these adsorbates on the Pb(111) surface can be fulfilled. We believe that our results constitute an important step for future experiments to perform high-resolution STM/AFM imaging with CO-terminated tips or the electronic decoupling of atoms and molecules from the prototypical Pb(111) superconducting surface.

Experimental

Sample preparation

The Pb(111) single crystal, purchased from Mateck GmbH, was cleaned by several sputtering and annealing cycles in ultra-high vacuum (UHV). CO dosing on the cold substrate was done in the

microscope chamber by increasing the pressure via a leak valve up to $p \approx 1\times10^{-7}$ mbar for one minute. This leads to a surface coverage of about 0.1-0.3 monolayer, as we readily observed on noble metals such as Cu, Ag or Au [33,45]. Iron adatoms were evaporated in the microscope head on the substrate at a temperature below 15 K. NaCl was evaporated from a quartz crucible on samples kept at room temperature in the preparation chamber.

Low-temperature scanning tunneling microscope

The experiments were performed using a low-temperature STM/AFM microscope (T = 4.8 K) from Omicron GmbH in UHV ($p \approx 1\times10^{-10}$ mbar) operated with Nanonis RC5 electronics. The sensor is a tuning fork sensor in a qPlus design [46] operated in the frequency-modulation mode (resonance frequency $f_0 \approx 25$ kHz, spring constant $k \approx 1800$ N/m, quality factor $Q \approx 14000$, and oscillation amplitude $A \approx 0.5$ Å). The tip mounted to the qPlus sensor consists of a 25 μm-thick PtIr wire, shortened and sharpened with a focused ion beam. A clean and sharp Pb tip was then prepared at low temperature by repeated indentations into the surface. STM images were acquired in constant-current mode with the bias voltage applied to the tip. All experimental data were analysed by using Gwyddion [47].

Results and Discussion

CO adsorption on Pb(111) and Pb(110)

Figure 1 shows STM images of CO molecules adsorbed on Pb(111). With a lattice parameter of a_{Pb} = 4.95 Å, the height of mono-atomic steps of the Pb(111) surface is expected to be $h_{Pb} = a_{\mathrm{Pb}}/2\sqrt{3}$ = 1.4 Å. Experimentally, a pristine Pb(111) sample (Fig. 1a) shows after sputtering and annealing cycles typically steps of about $2 \times h_{Pb}$ = 2.7 Å, which thus corresponds to diatomic steps. We assume that this peculiar step height distribution results from quantum size effect of the Pb(111) surface [48]. On the terraces, hexagonal dark spots are visible by STM, whose diameters vary between 1.5 nm and 5 nm with an apparent depression of 0.14 Å. They result from the interference of bulk electrons with trapped subsurface Ar gas bubbles after sputtering [49,50].

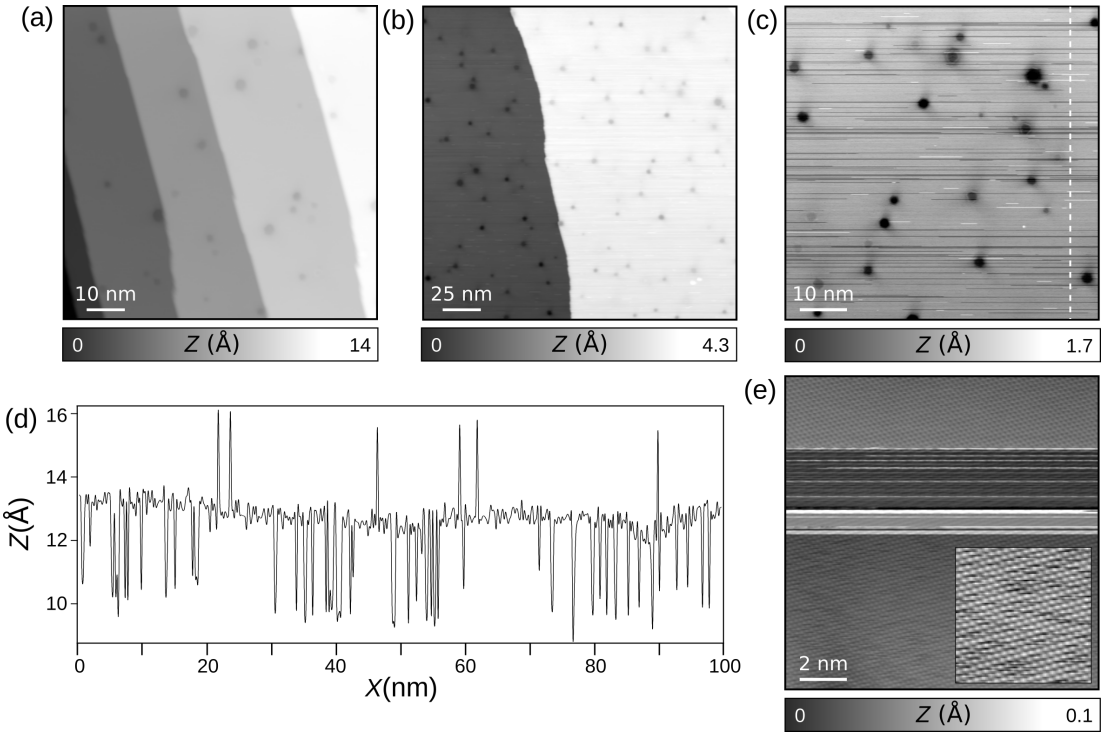

Figure 1: Carbon monoxide (CO) molecules adsorbed on Pb(111). (**a**) STM overview image of pristine Pb(111) (V_t = -0.1 V, I_t = 1 pA). (**b**) STM image after CO deposition. The estimated coverage is below 0.2 monolayer. (**c**) Close-up STM topography of CO molecules diffusing on the surface during scanning (V_t = -0.1 V, I_t = 40 pA). (**d**) Profile taken along the dashed white line of (**c**) showing spontaneous CO displacement under tip action. (**e**) Enhanced STM resolution (inset: more detailed image of the Pb(111) surface) resulting from the termination of the tip by a CO molecule (V_t = -0.2 V, I_t = 1 pA).

After CO dosing in the microscope chamber (see Sample preparation), a coverage of about 0.1-0.2 monolayer is expected to adsorb on the metal surface, as observed on different noble metals [33,45]. Figures 1b and c show STM topographic images after such process. While the surface topography remains unchanged in comparison to Figure 1a, numerous scan instabilities are now present which we attribute to CO molecules diffusing under gentle scan conditions (tunneling resistance of 200 GΩ). The STM profile (Figure 1d) taken along the white dashed line of Figure 1c shows several stochastic jumps, which we interpret as tip-induced displacements of single CO molecules [51-53]. We emphasize that the change of various scan parameters as well as tip indentations into the clean Pb surface were conducted to avoid such instabilities without noticeable improvements. Nevertheless, an unintentional CO-tip termination could be achieved as shown by the enhancement of the STM resolution in Figure 1e. In comparison to vertical manipulations of

CO on noble metals, we emphasize that CO-terminated tips on Pb(111) are much less stable, which severely limits the use of CO-terminated STM/AFM imaging on Pb(111). It should be noted that also other tip terminations are possible (such as with Xe), which we plan to explore in future work.

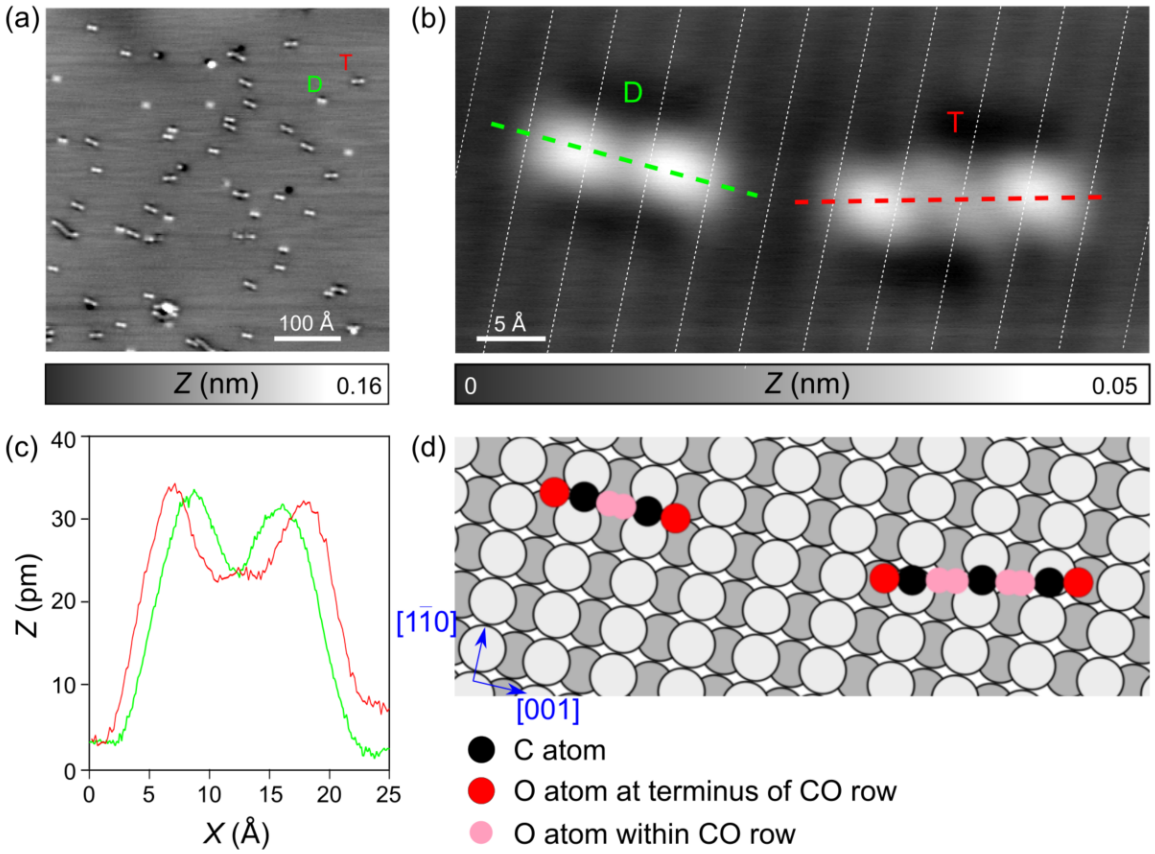

Figure 2: Adsorption of carbon monoxide (CO) molecules on Pb(110). (**a**) STM overview image of Pb(110) after adsorption of CO molecules (D: dimer, T: trimer, V_t = -0.5 V, I_t = 0.5 pA). (**b**) Closed-up STM image of a CO dimer and trimer (V_t = -0.1 V, I_t = 1 pA). (**c**) Profiles taken along the dashed lines of (**b**). (**d**) Sphere model of CO adsorbed on Pb(110). The CO molecules are standing up with protruding and tilted oxygen atoms (red, if tilted to chain terminus; pink, if tilted to center of CO chain), white and dark gray spheres refers to the topmost and downmost Pb atoms of the Pb(110) reconstruction.

Similar CO adsorptions were also conducted on Pb(110) (Figure 2a). There, most CO molecules appear in STM images as linear aggregates of different lengths, aligned nearly perpendicular to the [1$\bar{1}$0] row direction of Pb(110). The dimer-like protrusions ((*D*) in Figure 2b) exhibit a length of $\approx$ 7 Å between maxima (Figure 2c), corresponding to the distance of a_{Pb} = 4.95 Å between two Pb(110) rows (dashed lines in Figure 2b). The additional length of $\approx$ 2 Å might be related to the

tilting of the CO molecules under the scanning tip as well as the tip convolution during imaging. The trimeric protrusion (T) is rotated by about 16° compared to the [1$\bar{1}$0] rows. Its length of $\approx$ 11 Å corresponds to about three Pb(110) atomic rows, the additional length of $\approx$ 1 Å is again imputed to tilted CO during tip scanning. Last, these protrusions have a slight apparent depression around them, which might be related to a locally induced strain of the Pb lattice. While the D features are all aligned in the same direction, the orientation of the T features differs slightly. Both features have an apparent height of $\approx$ 0.3 Å, as extracted from the profile of Figure 2b, displayed in Figure 2c.

Overall, the CO adsorption on Pb(110) shows very strong similarities with adsorbed CO on Cu(110)-(2$\times$1)O as reported in references [54,55]. There, self-assembled CO molecules chemisorb with the C atom on top of Cu-O rows. According to DFT calculations, they lift the host Cu atom by 1 Å and the entire Cu-CO unit is tilted by $\approx \pm$ 45°. For measurements at 77 K, the two tilting configurations are supposed to convert rapidly, while at 4.5 K they are stable in one tilted configuration. At low coverages, CO adsorbed mostly as monomers and dimers, only occasionally trimers or even longer configurations were observed. Consecutive measurements showed however, that certain monomers formed dimers after some time. In STM the tilted CO molecules showed for each feature at the edges higher contrast as the interior molecules, which was explained by the different chemical environment. With this model, supported by DFT, reference [54] explained the formation of CO rows by dipole-dipole interactions, caused by the displacement of the Cu atom. They can be repulsive for vertical CO molecules [56,57], but attractive for tilted ones [54].

If we transfer this model to our measurements, the adsorption of the CO molecules might take place on top of the [1$\bar{1}$0] rows of the Pb(110) surface, as shown by the model in Figure 2d. For the dimer (D), the C atom is probably bonded to the Pb at the bridge sites of [1$\bar{1}$0] rows. The CO molecule is tilted similarly as on the Cu(110)-(2$\times$1)O surface [54,55] and appears in STM above the trenches of the Pb(110) surface. For the trimer (T), the mutual interaction of the interior CO molecules might cause a slight mismatch with the Pb(110) layer, which explains the small devi-

ation from the perpendicular alignment of the dimers. For longer CO aggregates, this deviation becomes even more apparent (see Figure 2a).

The reason, why CO can be observed with STM on Pb(110) and not on Pb(111) might be the fact, that in the [1$\bar{1}$0] rows of Pb(110) the attractive dipole-dipole interaction is initiated by a slight lift of the Pb atoms, which is not possible in the dense Pb(111) surface. It is also remarkable that the instability of the tilting angle of CO on Pb(110) at 4.5 K is comparable to that of CO on Cu(110)-(2×1)O at 77 K.

Growth of NaCl islands on Pb(111)

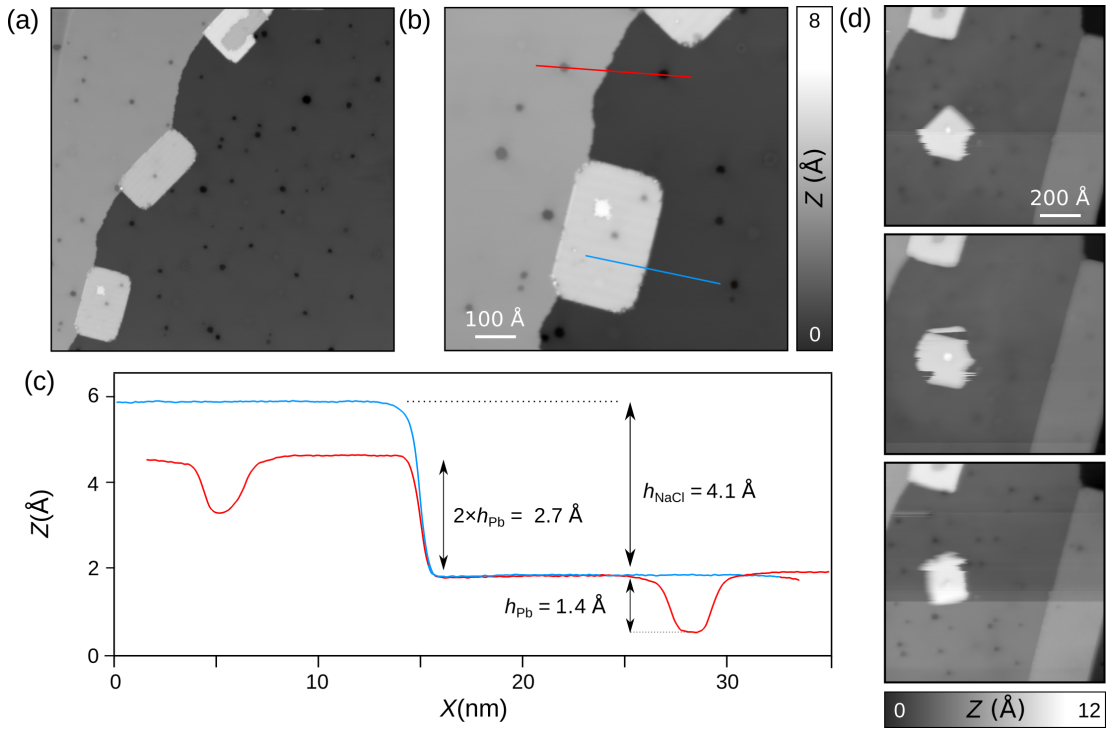

Figure 3: Adsorption of NaCl on Pb(111). (**a-b**) STM overview image of Pb(111) with quadratic NaCl islands adsorbed at step edges (V_t = -0.4 V, I_t = 1 pA). (**c**) Height profile extracted along the red and blue lines of (**b**). (**d**) Series of STM image showing the tip-induced rotation of an NaCl island (V_t = -0.4 V, I_t = 40 pA).

We next investigated the adsorption of NaCl on Pb(111) (Figure 3). Upon sublimation from a quartz crucible on a Pb(111) surface, which is kept at room temperature, NaCl forms without any post-annealing rectangular islands with round shaped corners attached to Pb step edges (Figures 3a and b). According to the profile, shown in Figure 3c, which is extracted along the red and blue

lines of Figure 1b, the step heights are equal to h_{NaCl} = 4.1 Å. This corresponds to a NaCl bilayer and is in agreement with the reported growth of NaCl islands on Cu(111) [58]. Occasionally, even a trilayer phase appears within the NaCl bilayer (Figures 3a and b). Note also that dark protrusions originating from trapped Ar atoms are still visible through the NaCl island by STM. Figure 3d shows series of consecutive STM images of a NaCl island adsorbed on a terrace. Upon scanning with a tunneling resistance of about 10 GΩ, the entire island rotates under the tip action around a trilayer signature as pinning center. This is in contrast to those NaCl islands, which are pinned to step edges. They remain always stable at T = 4.8 K, independent of the scanning conditions. As is, these islands exhibit characteristics similar to the ones on conventional metals [41,43,44] and thus they are likely adequate for the electronic decoupling of single atoms or molecules from the superconducting Pb(111).

Single Fe atoms on Pb(111) and their lateral manipulations

Figure 4 shows the deposition and controlled lateral manipulation of Fe adatoms on Pb(111). Upon deposition of Fe atoms on Pb(111) (kept below 15 K), several circular protrusions of different sizes and heights are observed by STM (Figure 4a). Their lateral sizes range from 0.3 to 1.5 Å, whereas their heights exhibit values of 0.4, 1.2 and 1.7 Å. Although no atomic resolution of these aggregates has been obtained, we interpret the variation of heights as a fingerprint for a Fe monomer, dimer and trimer, respectively (denoted as Fe_1, Fe_2 and Fe_3 in the following).

To confirm this assumption, we laterally manipulated single Fe adatoms with the STM tip [59,60] to intentionally form dimers and trimers and measure their apparent STM heights. To do so, the STM tip was positioned above a single Fe atom. The resistance of the STM junction was then decreased from about 50 GΩ (imaging) to 3 GΩ (manipulation) in order to trap the Fe atom in the STM junction [61]. Upon lateral tip displacements with a velocity of about 500 pm·s^{-1}, the trapped Fe atom is successfully displaced over the surface. During this process, a so-called "atom manipulation image" [34] can be obtained from such dragging of the Fe atom over Pb(111) (Figure 4b). The geometric features resemble typical patterns observed in friction force microscopy

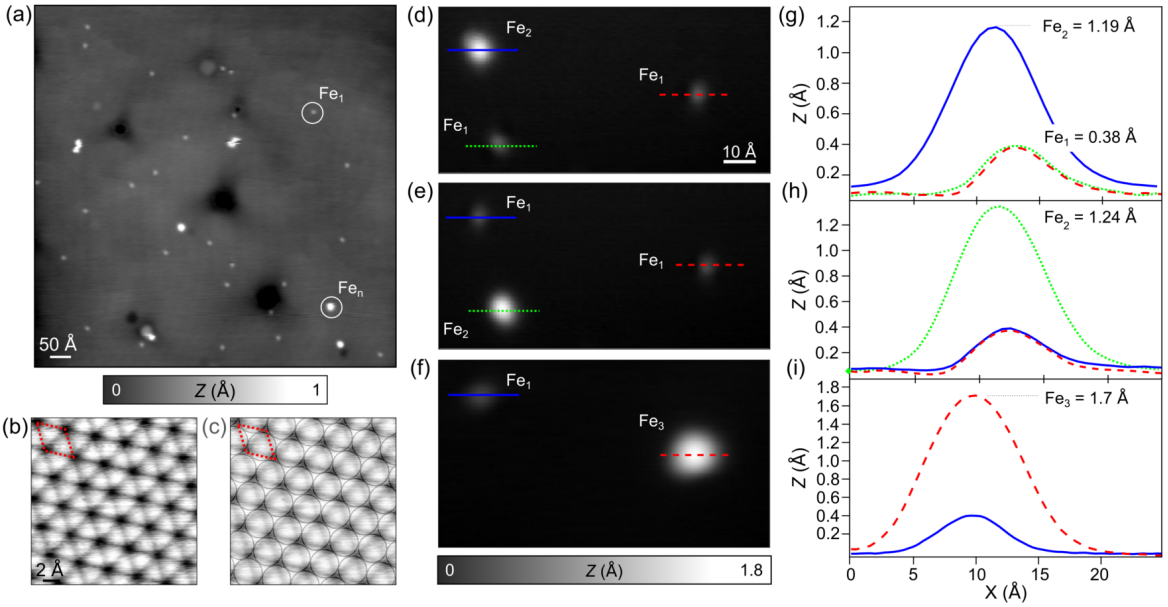

Figure 4: Fe adatoms on Pb(111) and their lateral manipulations. (a) STM overview image of Pb(111) after deposition of Fe adatoms (V_t = -700 mV, I_t = 5 pA). Fe_1 and Fe_n correspond to single Fe adatom and clusters of n adatoms, respectively (V_t = -15 mV, I_t = 5 pA). (b) Topographic STM image during the manipulation of a single Fe atoms trapped in the STM junction. (c) Models of the Pb(111) corresponding to the STM image of (b). The red dashed parallelogram refers to the Pb(111) lattice. (d-f) Series of STM images of Fe adatoms and their successive lateral manipulations with the STM tip (marked by arrows in (d) and (e)). In (f), the STM image shows the formation of a Fe-trimer Fe_3 by successive tip manipulations (Imaging conditions, V_t = -30 mV, I_t = 60 pA). (g-i) Apparent STM heights extracted from images (d-f) enabling one to distinguish from their topographic signatures Fe_1, Fe_2 and Fe_3, respectively.

(FFM) [28,29], since the trapped Fe atom senses the surface potential in analogy to the probing tip of FFM. For clarity, we overlay the Pb(111) surface lattice on top of the image in Figure 4c. The darkest features are spaced by 0.35 Å in agreement with the lattice parameters of Pb(111) and likely correspond to hollow sites, where the adatom preferentially is located.

Using this method, we transferred single atoms between different Fe clusters. In Figure 4d, two Fe single atoms (Fe_1) and an assumed dimer (Fe_2) are displayed. Figure 4g shows the corresponding apparent STM heights, which can be extracted from the lain, dotted and dashed lines of Figure 4d. Thus, we infer the heights of Fe_1 and Fe_2 aggregates to be $h_1 \approx 0.4$ Å and $h_2 \approx 1.2$ Å, respectively. As a verification, we then conducted the transfer of a single Fe atom (shown by the arrow in Figure 4d) from the Fe_2 cluster to one surrounding Fe_1 in order to form a new dimer. The result of

such manipulation is shown in Figure 4e. Despite the exchange of Fe atoms by tip manipulation, the apparent height of Fe_1 and Fe_2 remains identical as demonstrated by the STM profile of Figure 4h.

Finally, we brought by two successive tip manipulations the atoms of Fe_2 in Figure 4e to a third single atom (see arrow). The resulting image (Figure 4f) reveals the formation of a Fe-trimer (Fe_3). Compared to the heights of Fe_1 and Fe_2, the Fe_3 height is about h_3 = 1.7 Å. This evolution of STM apparent heights as a function of number of atoms in small Fe clusters is in good agreement with a similar study of Fe clusters on Cu(111) [62].

Conclusion

Our results report on the systematic characterization by STM of the adsorption of carbon monoxide (CO), sodium chloride (NaCl) and iron adatoms (Fe) on the superconducting Pb(111) surface at low temperature (4.7 K). We show a surprising absence of STM topographic signatures of CO molecules on Pb(111), which we impute to their high propensity of diffusing under gentle scanning conditions. In contrast, CO molecules become apparent by STM on Pb(110), since they initiate attractive dipole-dipole interactions, which support the formation of linear aggregates. Furthermore, we show that deposition of NaCl on Pb(111) leads to bilayer islands similar to literature data. Lastly, cold-temperature deposition ($\leq$ 15 K) of Fe on Pb(111) leads to the adsorption of adatoms and small Fe clusters. Using tip-induced lateral manipulations, we demonstrate the exchange of Fe single atoms between these clusters and characterize the variation of apparent STM height of each cluster as a function of the number of atoms. Overall, our findings provide new insights into high-resolution STM/AFM imaging with functionalized tips, decoupling of atoms or molecules and tip-induced lateral manipulation of Fe atoms above the prototypical Pb(111) superconducting surface.

Acknowledgements

Financial support from the Swiss National Science Foundation (SNF) and the Swiss Nanoscience Institute (SNI) is gratefully acknowledged. We also thank the European Research Council (ERC)

under the European Union's Horizon 2020 research and innovation programme (ULTRADISS Grant Agreement No. 834402).

References

1. Nayak, C.; Simon, S. H.; Stern, A.; Freedman, M.; Das Sarma, S. *Reviews of Modern Physics* **2008**, *80*, 1083–1159. doi:10.1103/RevModPhys.80.1083.

2. Sato, M.; Ando, Y. *Reports on Progress in Physics* **2017**, *80*, 076501. doi:10.1088/1361-6633/aa6ac7.

3. Frolov, S. M.; Manfra, M. J.; Sau, J. D. *Nature Physics* **2020**, *16* (7), 718–724. doi:10.1038/s41567-020-0925-6.

4. Majorana, E. *Il Nuovo Cimento* **1937**, *14*, 171. doi:10.1007/BF02961314.

5. Kitaev, A. Y. *Physics-Uspekhi* **2001**, *44* (10S), 131–136. doi:10.1070/1063-7869/44/10s/s29.

6. Alicea, J. *Reports on Progress in Physics* **2012**, *75* (7), 076501. doi:10.1088/0034-4885/75/7/076501.

7. Wang, Z.; Rodriguez, J. O.; Jiao, L.; Howard, S.; Graham, M.; Gu, G. D.; Hughes, T. L.; Morr, D. K.; Madhavan, V. *Science* **2020**, *367*, 104–108. doi:10.1126/science.aaw8419.

8. Lutchyn, R. M.; Bakkers, E. P. A. M.; Kouwenhoven, L. P.; Krogstrup, P.; Marcus, C. M.; Oreg, Y. *Nature Reviews Materials* **2018**, *3*, 52–68. doi:10.1038/s41578-018-0003-1.

9. Mourik, V.; Zuo, K.; Frolov, S. M.; Plissard, S. R.; Bakkers, E. P. A. M.; Kouwenhoven, L. P. *Science* **2012**, *336*, 1003. doi:10.1126/science.1222360.

10. Nadj-Perge, S.; Drozdov, I. K.; Bernevig, B. A.; Yazdani, A. *Physical Review B* **2013**, *88* (2), 020407. doi:10.1103/PhysRevB.88.020407.

11. Pientka, F.; Glazman, L. I.; von Oppen, F. *Physical Review B* **2013**, *88* (15), 155420. doi:10.1103/PhysRevB.88.155420.

12. Klinovaja, J.; Stano, P.; Yazdani, A.; Loss, D. *Physical Review Letters* **2013**, *111* (18), 186805. doi:10.1103/PhysRevLett.111.186805.

13. Nadj-Perge, S.; Drozdov, I. K.; Li, J.; Chen, H.; Jeon, S.; Seo, J.; MacDonald, A. H.; Bernevig, B. A.; Yazdani, A. *Science* **2014**, *346* (6209), 602–607. doi:10.1126/science.1259327.

14. Ruby, M.; Pientka, F.; Peng, Y.; von Oppen, F.; Heinrich, B. W.; Franke, K. J. *Phys. Rev. Lett.* **2015**, *115*, 197204. doi:10.1103/PhysRevLett.115.197204.

15. Pawlak, R.; Kisiel, M.; Klinovaja, J.; Meier, T.; Kawai, S.; Glatzel, T.; Loss, D.; Meyer, E. *npj Quantum Information* **2016**, *2* (16035), year. doi:10.1038/npjqi.2016.35.

16. Kim, H.; Palacio-Morales, A.; Posske, T.; Rózsa, L.; Palotás, K.; Szunyogh, L.; Thorwart, M.; Wiesendanger, R. *Science Advances* **2018**, *4* (5), year. doi:10.1126/sciadv.aar5251.

17. Jäck, B.; Xie, Y.; Li, J.; Jeon, S.; Bernevig, B. A.; Yazdani, A. *Science* **2019**, *364*, 1255–1259. doi:10.1126/science.aax1444.

18. Palacio-Morales, A.; Mascot, E.; Cocklin, S.; Kim, H.; Rachel, S.; Morr, D. K.; Wiesendanger, R. *Science Advances* **2019**, *5*, eaav6600. doi:10.1126/sciadv.aav6600.

19. Fu, L.; Kane, C. L. *Physical Review Letters* **2008**, *100*, 096407. doi:10.1103/PhysRevLett.100.096407.

20. Sun, H.-H.; Zhang, K.-W.; Hu, L.-H.; Li, C.; Wang, G.-Y.; Ma, H.-Y.; Xu, Z.-A.; Gao, C.-L.; Guan, D.-D.; Li, Y.-Y.; Liu, C.; Qian, D.; Zhou, Y.; Fu, L.; Li, S.-C.; Zhang, F.-C.; Jia, J.-F. *Physical Review Letters* **2016**, *116*, 257003. doi:10.1103/PhysRevLett.116.257003.

21. Zhang, P.; Yaji, K.; Hashimoto, T.; Ota, Y.; Kondo, T.; Okazaki, K.; Wang, Z.; Wen, J.; Gu, G. D.; Ding, H.; Shin, S. *Science* **2018**, *360*, 182–186. doi:10.1126/science.aan4596.

22. Zhu, S.; Kong, L.; Cao, L.; Chen, H.; Papaj, M.; Du, S.; Xing, Y.; Liu, W.; Wang, D.; Shen, C.; Yang, F.; Schneeloch, J.; Zhong, R.; Gu, G.; Fu, L.; Zhang, Y.-Y.; Ding, H.; Gao, H.-J. *Science* **2020**, *367*, 189–192. doi:10.1126/science.aax0274.

23. Kezilebieke, S.; Huda, M. N.; Vaňo, V.; Aapro, M.; Ganguli, S. C.; Silveira, O. J.; Głodzik, S.; Foster, A. S.; Ojanen, T.; Liljeroth, P. *Nature* **2020**, *588* (7838), 424–428. doi:10.1038/s41586-020-2989-y.

24. Bartels, L.; Meyer, G.; Rieder, K.-H. *Applied Physics Letters* **1997**, *71* (2), 213–215. doi:10.1063/1.119503.

25. Gross, L.; Mohn, F.; Moll, N.; Liljeroth, P.; Meyer, G. *Science* **2009**, *325* (5944), 1110–1114. doi:10.1126/science.1176210.

26. Gross, L. *Nature Chemistry* **2011**, *3* (4), 273–278. doi:10.1038/nchem.1008.

27. Stroscio, J. A.; Eigler, D. M. *Science* **1991**, *254* (5036), 1319–1326. doi:10.1126/science.254.5036.1319.

28. Pawlak, R.; Ouyang, W.; Filippov, A. E.; Kalikhman-Razvozov, L.; Kawai, S.; Glatzel, T.; Gnecco, E.; Baratoff, A.; Zheng, Q.; Hod, O.; Urbakh, M.; Meyer, E. *ACS Nano* **2016**, *10* (1), 713–722. doi:10.1021/acsnano.5b05761.

29. Pawlak, R.; Kawai, S.; Meier, T.; Glatzel, T.; Baratoff, A.; Meyer, E. *Journal of Physics D: Applied Physics* **2017**, *50* (11), 113003. doi:10.1088/1361-6463/aa599d.

30. Kawai, S.; Koch, M.; Gnecco, E.; Sadeghi, A.; Pawlak, R.; Glatzel, T.; Schwarz, J.; Goedecker, S.; Hecht, S.; Baratoff, A.; Grill, L.; Meyer, E. *Proceedings of the National Academy of Sciences* **2014**, *111* (11), 3968–3972. doi:10.1073/pnas.1319938111.

31. Kawai, S.; Benassi, A.; Gnecco, E.; Söde, H.; Pawlak, R.; Feng, X.; Müllen, K.; Passerone, D.; Pignedoli, C. A.; Ruffieux, P.; Fasel, R.; Meyer, E. *Science* **2016**, *351* (6276), 957–961. doi:10.1126/science.aad3569.

291 32. Pawlak, R.; Vilhena, J. G.; Hinaut, A.; Meier, T.; Glatzel, T.; Baratoff, A.; Gnecco, E.;
292 Pérez, R.; Meyer, E. *Nature Communications* **2019**, *10* (1), 685. doi:10.1038/
293 s41467-019-08531-4.

294 33. Pawlak, R.; Vilhena, J. G.; D'Astolfo, P.; Liu, X.; Prampolini, G.; Meier, T.; Glatzel, T.;
295 Lemkul, J. A.; Häner, R.; Decurtins, S.; Baratoff, A.; Pérez, R.; Liu, S.-X.; Meyer, E. *Nano*
296 *Letters* **2020**, *20* (1), 652–657. doi:10.1021/acs.nanolett.9b04418.

297 34. Celotta, R. J.; Balakirsky, S. B.; Fein, A. P.; Hess, F. M.; Rutter, G. M.; Stroscio, J. A. *Review*
298 *of Scientific Instruments* **2014**, *85* (12), 121301. doi:10.1063/1.4902536.

299 35. Khajetoorians, A. A.; Wegner, D.; Otte, A. F.; Swart, I. *Nature Reviews Physics* **2019**, *1* (12),
300 703–715. doi:10.1038/s42254-019-0108-5.

301 36. Nadj-Perge, S.; Drozdov, I. K.; Li, J.; Chen, H.; Jeon, S.; Seo, J.; MacDonald, A. H.;
302 Bernevig, B. A.; Yazdani, A. *Science* **2014**, *346* (6209), 602–607. doi:10.1126/science.
303 1259327.

304 37. Feldman, B. E.; Randeria, M. T.; Li, J.; Jeon, S.; Xie, Y.; Wang, Z.; Drozdov, I. K.; An-
305 drei Bernevig, B.; Yazdani, A. *Nature Physics* **2017**, *13*, 286–291. doi:10.1038/nphys3947.

306 38. Kamlapure, A.; Cornils, L.; Wiebe, J.; Wiesendanger, R. *Nature Communications* **2018**, *9* (1),
307 3253. doi:10.1038/s41467-018-05701-8. Number: 1 Publisher: Nature Publishing Group

308 39. Heinrich, B. W.; Braun, L.; Pascual, J. I.; Franke, K. J. *Nature Physics* **2013**, *9* (12), 765–768.
309 doi:10.1038/nphys2794.

310 40. Heinrich, B. W.; Braun, L.; Pascual, J. I.; Franke, K. J. *Nano Letters* **2015**, *15* (6), 4024–4028.
311 doi:10.1021/acs.nanolett.5b00987.

312 41. Repp, J.; Meyer, G.; Stojković, S. M.; Gourdon, A.; Joachim, C. *Physical Review Letters*
313 **2005**, *94* (2), 026803. doi:10.1103/PhysRevLett.94.026803.

42. Hirjibehedin, C. F.; Lutz, C. P.; Heinrich, A. J. *Science* **2006**, *312* (5776), 1021–1024. doi:10.1126/science.1125398.

43. Repp, J.; Steurer, W.; Scivetti, I.; Persson, M.; Gross, L.; Meyer, G. *Physical Review Letters* **2016**, *117* (14), 146102. doi:10.1103/PhysRevLett.117.146102.

44. Meier, T.; Pawlak, R.; Kawai, S.; Geng, Y.; Liu, X.; Decurtins, S.; Hapala, P.; Baratoff, A.; Liu, S.-X.; Jelínek, P.; Meyer, E.; Glatzel, T. *ACS Nano* **2017**, *11* (8), 8413–8420. doi:10.1021/acsnano.7b03954.

45. Pawlak, R.; Drechsel, C.; D'Astolfo, P.; Kisiel, M.; Meyer, E.; Cerda, J. I. *Proceedings of the National Academy of Sciences* **2020**, *117* (1), 228–237. doi:10.1073/pnas.1913489117.

46. Giessibl, F. J. *Reviews of Modern Physics* **2003**, *75* (3), 949–983. doi:10.1103/RevModPhys.75.949.

47. Nečas, D.; Klapetek, P. *Open Physics* **2012**, *10* (1), 181–188. doi:10.2478/s11534-011-0096-2.

48. Chang, S. H.; Su, W. B.; Jian, W. B.; Chang, C. S.; Chen, L. J.; Tsong, T. T. *Physical Review B* **2002**, *65* (24), 245401. doi:10.1103/PhysRevB.65.245401.

49. Schmid, M.; Hebenstreit, W.; Varga, P.; Crampin, S. *Phys. Rev. Lett.* **1996**, *76*, 2298–2301. doi:10.1103/PhysRevLett.76.2298.

50. Song, S. Y.; Seo, J. *Scientific Reports* **2017**, *7* (1), 12177. doi:10.1038/s41598-017-12505-1.

51. Auwärter, W.; Seufert, K.; Bischoff, F.; Ecija, D.; Vijayaraghavan, S.; Joshi, S.; Klappenberger, F.; Samudrala, N.; Barth, J. V. *Nature Nanotechnology* **2012**, *7* (1), 41–46. doi:10.1038/nnano.2011.211.

52. Choi, D.-J.; Rubio-Verdú, C.; de Bruijckere, J.; Ugeda, M. M.; Lorente, N.; Pascual, J. I. *Nature Communications* **2017**, *8* (1), 15175. doi:10.1038/ncomms15175.

337 53. Fremy-Koch, S.; Sadeghi, A.; Pawlak, R.; Kawai, S.; Baratoff, A.; Goedecker, S.; Meyer, E.;
338 Glatzel, T. *Physical Review B* **2019**, *100* (15), 155427. doi:10.1103/PhysRevB.100.155427.

339 54. Feng, M.; Cabrera-Sanfelix, P.; Lin, C.; Arnau, A.; Sánchez-Portal, D.; Zhao, J.;
340 Echenique, P. M.; Petek, H. *ACS Nano* **2011**, *5* (11), 8877–8883. doi:10.1021/nn203041c.
341 Publisher: American Chemical Society

342 55. Feng, M.; Lin, C.; Zhao, J.; Petek, H. *Annu. Rev. Phys. Chem.* **2012**, *63* (1), 201–224. doi:10.
343 1146/annurev-physchem-032210-103353.

344 56. Ahner, J.; Mocuta, D.; Ramsier, R. D.; Yates, J. T. *The Journal of Chemical Physics* **1996**, *105*
345 (15), 6553–6559. doi:10.1063/1.472464. Publisher: American Institute of Physics

346 57. Kato, H.; Okuyama, H.; Ichihara, S.; Kawai, M.; Yoshinobu, J. *The Journal of Chemical*
347 *Physics* **2000**, *112* (4), 1925–1936. doi:10.1063/1.480771. Publisher: American Institute of
348 Physics

349 58. Repp, J.; Meyer, G.; Rieder, K.-H. *Physical Review Letters* **2004**, *92* (3), 036803. doi:10.1103/
350 PhysRevLett.92.036803.

351 59. Hla, S.-W.; Braun, K.-F.; Rieder, K.-H. *Physical Review B* **2003**, *67* (20), 201402. doi:
352 10.1103/PhysRevB.67.201402.

353 60. Hla, S.-W. *Journal of Vacuum Science & Technology B: Microelectronics and Nanome-*
354 *ter Structures Processing, Measurement, and Phenomena* **2005**, *23* (4), 1351–1360. doi:
355 10.1116/1.1990161.

356 61. Bartels, L.; Meyer, G.; Rieder, K.-H. *Physical Review Letters* **1997**, *79* (4), 697–700. doi:10.
357 1103/PhysRevLett.79.697.

358 62. Emmrich, M.; Huber, F.; Pielmeier, F.; Welker, J.; Hofmann, T.; Schneiderbauer, M.;
359 Meuer, D.; Polesya, S.; Mankovsky, S.; Ködderitzsch, D.; Ebert, H.; Giessibl, F. J. *Science*
360 **2015**, *348* (6232), 308–311. doi:10.1126/science.aaa5329.